Scientia Iranica D (2015) 22(6), 2505–2515

SCIENTIA IRANICA

Sharif University of Technology

Scientia Iranica

Transactions D: Computer Science & Engineering and Electrical Engineering

www.scientiairanica.com

A new control method for grid-connected quasi-Z-source multilevel inverter based photovoltaic system

A. Akhavan* and H.R. Mohammadi

Department of Electrical Engineering, University of Kashan, Kashan, Iran.

Received 19 November 2014; received in revised form 5 June 2015; accepted 22 June 2015

KEYWORDS

Quasi-Z-source inverter;
Cascaded multilevel inverter;
Photovoltaic system;
Particle swarm optimization;
Artificial neural network.

Abstract. In this paper, a new control method for quasi-Z-source cascaded multilevel inverter based grid-connected photovoltaic (PV) system, using evolutionary algorithm and Artificial Neural Network (ANN), is proposed. The proposed method is capable of boosting the PV array voltage to a higher level and it solves the imbalanced problem of DC-link voltage in traditional cascaded H-bridge inverters using ANN. The proposed control system adjusts the grid injected current in phase with the grid voltage and achieves independent Maximum Power Point Tracking (MPPT) for the separate PV arrays by Proportional-Integral (PI) controllers. For achieving the best performance, this paper presents an optimum approach to design the controller parameters using Particle Swarm Optimization (PSO). The primary design goal is to obtain good response by minimizing the integral absolute error. Also, the transient response is guaranteed by minimizing the overshoot, settling time, and rise time of the system response. Effectiveness of the new proposed control method has been verified through simulation studies in a seven-level quasi-Z-source cascaded multilevel inverter.

1. Introduction

Photovoltaic (PV) power generation has a great potential to serve as a clean and inexhaustible renewable energy source. However, output power of the PV arrays is greatly affected by environmental conditions, such as stochastic changes of the temperature and solar irradiance. In PV systems, extracting the maximum power of the PV array and current injection into the grid at unity power factor are necessary. In recent years, applying various multilevel inverter topologies to PV systems is getting more and more attention due to the large power-scale and high voltage demands. Among various topologies, Cascaded H-Bridge (CHB) inverter has unique advantages and has been identified as a suitable topology for transformer-less, grid-connected PV systems [1]. Applying CHB inverter in the PV systems has some advantages, such as the independent Maximum Power Point Tracking (MPPT) of each array. However, the DC-link voltage in each inverter module is not constant, because PV array voltage varies with changes of environmental conditions, such as temperature and solar irradiation or partial shadows. These cases will cause an unbalanced DC-link voltage among different H-bridge modules. Furthermore, in the conventional Cascaded Multilevel Inverter (CMI) based PV system, each module is a buck inverter because the first component of the output AC voltage is always lower than the input DC voltage. Therefore, an additional DC-DC boost converter is necessary to obtain the desired output voltage and also to balance the DC-link voltages. This DC-DC boost

*. *Corresponding author. Tel.: +98 3155333908*
E-mail addresses: aliakhavan1369@gmail.com (A. Akhavan); mohammadi@kashanu.ac.ir (H.R. Mohammadi)

converter increases the complexity of the power and control circuit and reduces the efficiency [2-5].

In recent years, the Z-Source Inverter (ZSI) and Quasi-Z-Source Inverter (QZSI) have been employed for the PV power generation system due to some unique advantages and features. The ZSI has a discontinuous input current during the shoot-through state due to presence of the blocking diode [6-8]. Thus, this configuration is not appropriate for photovoltaic applications. Nowadays, Quasi-Z-Source Cascaded Multilevel Inverter (QZS-CMI) based PV systems were proposed which have continuous input current and boosting capability and also inherit the advantages of traditional CMI, while overcoming issues with imbalanced DC-link voltages among independent modules [9,10]. Liu et al. [2] use PI controllers for designing the whole control system; but in the presented control method, each QZS-CMI module needs a control loop for DC-link peak voltage control which causes the complexity of the control system. Several works are done related to QZS-CMI, for example: Liu et al. [11], Shajith and Kamaraj [12], and Sun et al. [13] present the various multi-carrier bipolar PWM techniques for QZS-CMI and Liu et al. [14], and Sun et al. [15] focus on parameter design of the QZS-CMI. The Phase Shifted Sinusoidal Pulse Width Modulation (PS-SPWM) is used as a modulation scheme for QZS-CMI in [16].

In this paper, a new control method for a QZS-CMI based PV system is proposed. The control objectives are independent DC-link voltage control, independent MPPT control, and current injection into the grid at unity power factor. The Artificial Neural Network (ANN) and PI controllers are employed to control QZS-CMI. The independent DC-link voltage control is achieved using ANN. Applying the ANN has some advantages in comparison to using PI controllers in [2]. In this method, the DC-link peak voltage control loop for each module is removed and only one ANN is used for all modules, which causes simplicity in the control system and cost reduction. Also, PI controllers have a delay time due to integral term. Consequently, by removing the PI controllers in the DC-link peak voltage control loop and using ANN, the delay time decreases in the transient conditions. Besides, the reliability of the control system enhances using ANN. In fact, if any input data is out of range due to failing in the measurements, the ANN gets acceptable outputs. In this paper, the independent MPPT and current injection are controlled using PI controllers. There have been many technical methods for designing the control parameters in the time and frequency domain. Mostly, design of control parameters using these methods are time-consuming. To achieve a high and fast performance, this paper presents an optimum approach to design PI parameters using Particle Swarm Optimization (PSO). In the PSO method, the primary goal for the design of control parameters is to obtain good steady state response by minimizing the integral absolute error. Also, the transient response is guaranteed by minimizing the overshoot, settling time, and rise time of the system response. In fact, the objective function is defined so that both the steady state and transient response improve. Also, the PS-SPWM modulation scheme is used for the QZS-CMI. This paper is organized as follows: Section 2 consists of an overview of the system with the proposed control strategy; Section 3 focuses on the system modeling and grid-connected control; design of the PI parameters using PSO is presented in Section 4; the PS-SPWM modulation scheme is presented in Section 5; effectiveness of the proposed control strategy is verified by simulation in PSCAD/EMTDC software and the results are compared with the results of reference [2] in Section 6; and finally, a conclusion is made in Section 7.

2. QZS-CMI and its control strategy

The QZS-CMI based grid-connected PV system with the proposed control strategy is shown in Figure 1. Comparing to the conventional CMI module, an inductor-capacitor impedance network is included in the input stage of each module. This structure is used to synthesize DC voltage sources to generate $2n+1$ staircase output waveform, wherein n is the number of independent PV array.

2.1. Quasi-Z-source inverter operation

The QZS-CMI combines the QZS network into each CMI module. The QZSI can be operated in two modes, i.e. the non-shoot-through and the shoot-through [16]. Figure 2 shows the QZSI equivalent circuits operating in the two modes and defines the polarities of all voltages and currents. If the switching period, shoot-through period, and non-shoot-through period are considered as T_s, T_{sh}, and T_{nsh}, respectively, the Eq. (1) can be written as:

$$T_s = T_{sh} + T_{nsh}. \tag{1}$$

Therefore, the shoot-through duty ratio is $D = T_{sh}/T_s$. When the kth module is in non-shoot-through state, the power is transmitted from the DC side to the AC side and the inverter operates as a traditional CMI. In steady state, the following relations can be obtained [2]:

$$\hat{V}_{DCk} = \frac{1}{1-2D_k} V_{PVk} = B_k V_{PVk},$$

$$V_{Hk} = S_k \hat{V}_{DCk}. \tag{2}$$

While in a shoot-through mode, there is no power transmission, because the DC-link voltage is zero. In this mode, there are:

$$\hat{V}_{DCk} = 0, \qquad V_{Hk} = 0. \tag{3}$$

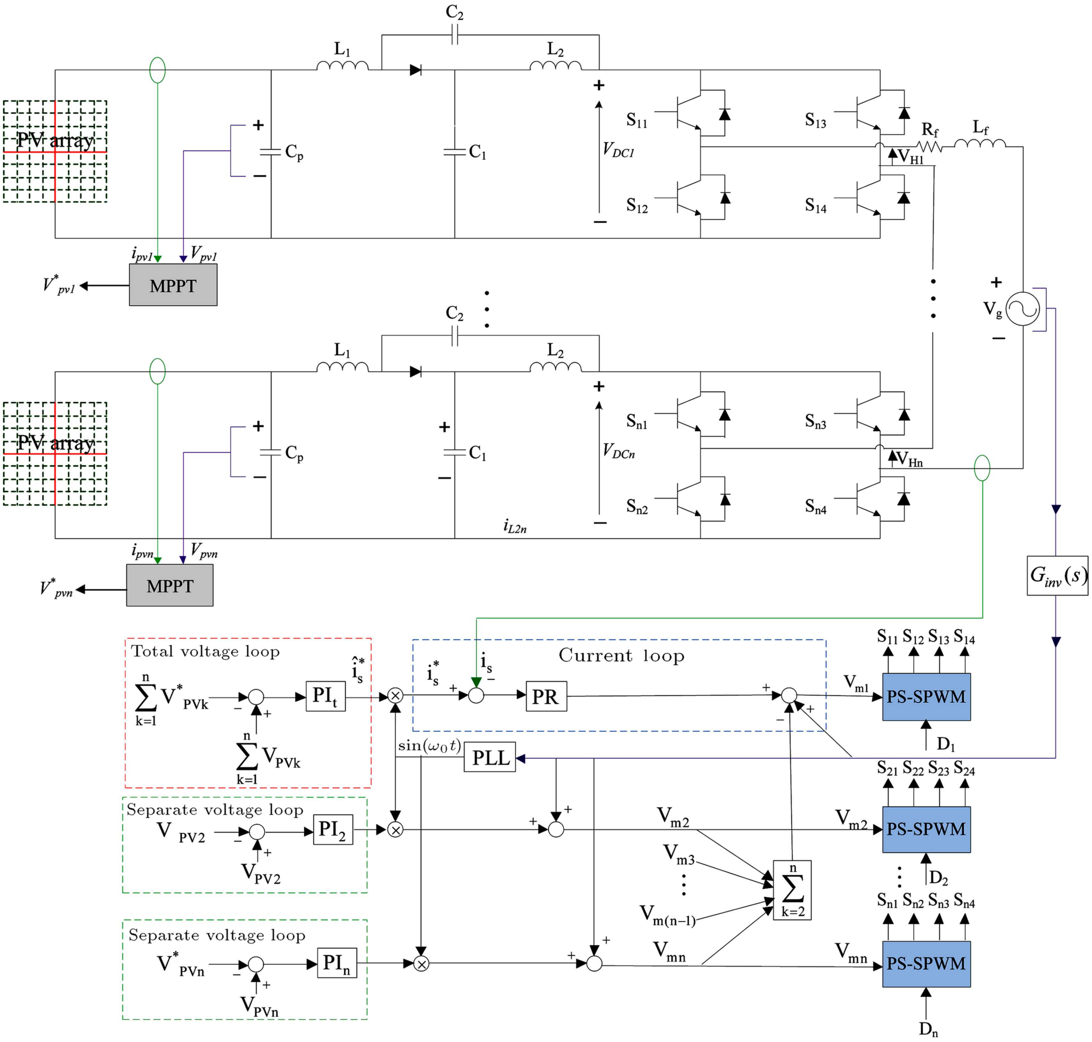

(a)

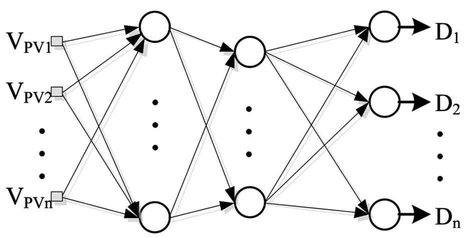

(b)

Figure 1. (a) QZS-CMI based grid-connected PV power system. (b) ANN structure for dc-link peak voltage control.

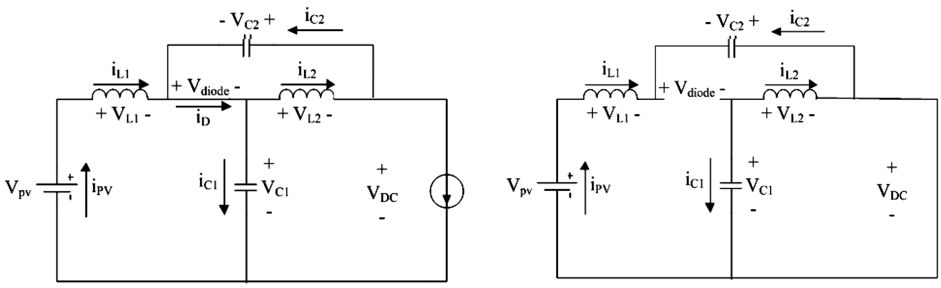

(a) (b)

Figure 2. The equivalent circuit of the QZSI: (a) Non-shoot-through state; and (b) shoot-through state.

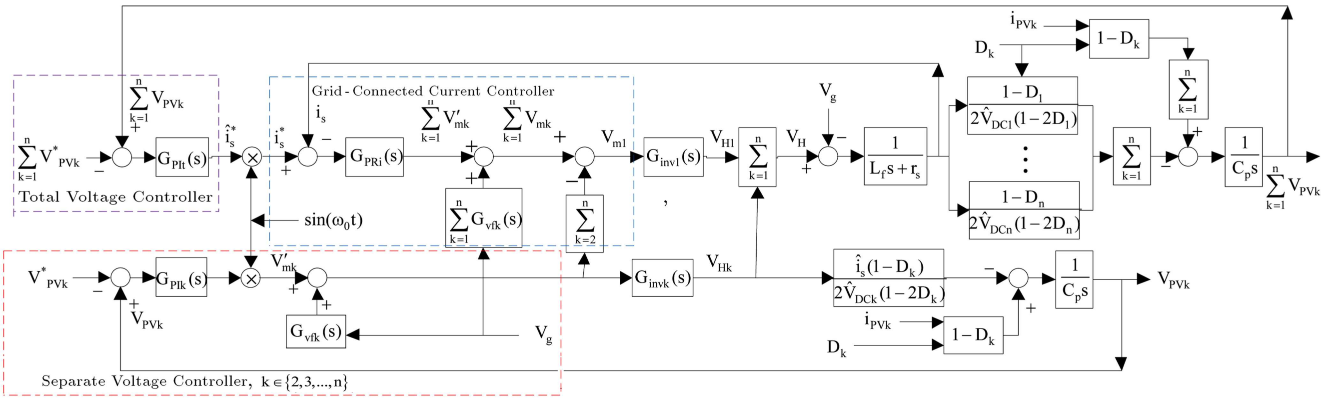

Figure 3. Block diagram of the proposed control grid-connected system for the QZS-CMI based PV system.

For the QZS-CMI, the output synthesized voltage is equal to:

$$V_H = \sum_{k=1}^{n} V_{Hk} = \sum_{k=1}^{n} S_k \hat{V}_{DCk}. \quad (4)$$

In the above equations, $\hat{V}_{DCk}$ is the kth module DC-link peak voltage; V_{PVk} is the output voltage of the kth PV array; D_k and B_k are the shoot-through duty ratio and boost factor of the kth module, respectively; V_{Hk} is the output voltage of the kth module and $S_k \in \{-1,\ 0,\ 1\}$ is the switching function of the kth module.

2.2. Principle of control strategy

Each QZS-CMI module has two independent control commands: shoot-through duty ratio, D_k, and modulation signal, V_{mk}. D_k is used to adjust the DC-link voltage to a desired reference value, while V_{mk} is used to control the grid injected power. The main goals of the control system of QZS-CMI based grid-connected PV system are: 1) Independent MPPT for each module to ensure the maximum power extraction from each PV array; 2) Current injection into the grid at unity power factor; and 3) Balanced DC-link peak voltage for all QZS-CMI modules.

To achieve these goals, the PI controllers and ANN are employed. The total PV array voltage loop adjusts the sum of n PV array voltages using a PI controller, PI_t. Each PV array voltage reference is calculated by its MPPT block. Also, the current loop achieves a sinusoidal grid-injected current in phase with the grid voltage. A Proportional-Resonant (PR) controller makes the actual grid-injected current to track its desired value [17]. The $n-1$ independent PV array voltage loops control the other $n-1$ PV array voltages to achieve their own MPPTs through the $n-1$ PI controllers, named as PI_2 to PI_n, respectively. Also, as shown in Figure 1(b), the DC-link peak voltage of each module is controlled by means of shoot-through duty ratio which is determined by an ANN. The inputs of ANN are the real PV array voltages and its outputs are the shoot-through duty ratios for the DC-link voltage control system. Finally, the shoot-through duty ratio D_k and modulation signal V_{mk} for kth module are combined into the PS-SPWM modulation scheme to achieve the desired goals.

3. System modeling

The block diagram of the QZS-CMI based grid-connected PV system is shown in Figure 3. The details will be explained as follows.

3.1. Independent PV voltage and injected current control

In the kth QZS-CMI module, the current of the inductor L_1 is:

$$i_{L1k} = i_{PVk} - C_p \frac{dV_{PVk}}{dt}, \quad (5)$$

where i_{L1k} is the current of inductor, L_1; i_{PVk} is the current of kth PV array; and C_p is the shunt capacitor with the PV array. The total output voltage of the QZS-CMI can be written as:

$$V_H = V_g + L_f \frac{di_s}{dt} + r_f i_s, \quad (6)$$

where V_g is the grid voltage and i_s is the grid injected current; r_f is parasitic resistance and L_f is the filter inductance. Consequently, the transfer function of the grid injected current can be obtained by:

$$G_f(s) = \frac{I_s(s)}{V_H(s) - V_g(s)} = \frac{1}{L_f s + r_f}. \quad (7)$$

To make the actual grid injected current track the desired reference, a PR controller $G_{PRi}(s) = k_{iP} + \frac{k_{iR}\omega_0}{s^2+\omega_0^2}$ is used, where ω_0 is the resonant frequency, i.e. 314 rad/s.

In the next step, a grid voltage feed-forward control loop is applied. Therefore, the kth module has the following modulation signal:

$$V_{mk} = V'_{mk} + V_g(s) G_{vfk}(s), \quad (8)$$

where, V_{mk} is the kth module modulation signal; V'_{mk} is output of the PI controller in the kth module, and $G_{vfk}(s)$ is as follows [2]:

$$G_{vfk}(s)=\frac{1}{nG_{invk}(s)},$$

$$G_{invk}(s)=\frac{V_{Hk}(s)}{V_{mk}(s)}=\hat{V}_{DCk}. \tag{9}$$

Due to DC-link peak voltage balance control, the DC-link peak voltages are equal. Therefore:

$$G_{invk}(s)=G_{inv}(s), \qquad k\in\{1,2,...,m\}. \tag{10}$$

According to Figure 3, the closed-loop transfer function of the grid injected current control system can be written in Eq. (11) as shown in Box I. According to Figure 1, each PV array voltage can be obtained by:

$$V_{PVk}(s)=\frac{1}{C_p s}\left[I_{PVk}(s)-I_{L1k}(s)\right]. \tag{12}$$

In the non-shoot-through mode, the output power is equal to input power [2]. Therefore:

$$\frac{\hat{i}_s\hat{v}_{Hk}}{2}=\hat{v}_{DCk}\bar{i}_{DCK}=\nu_{PVk}\bar{i}_{L1k\_nsh}. \tag{13}$$

In the above equation, $\hat{v}_{Hk}$ is the output peak voltage of the kth module; $\bar{i}_{DCk}$ is the average current of the DC-link in the kth module; $\bar{i}_{L1k\_nsh}$ is the average current of inductor L_1 in non-shoot-through mode. Eq. (13) can be rewritten using Eq. (2) as follows:

$$\bar{i}_{L1k\_nsh}=\frac{\hat{i}_s\hat{v}_{Hk}}{2\hat{v}_{DCk}(1-2D_k)}. \tag{14}$$

Also, in the shoot-through mode, the average current of the inductor L_1 is:

$$\bar{i}_{L1k\_sh}=i_{PVk}. \tag{15}$$

Therefore, the average current of the inductor L_1 in the one switching cycle can be obtained as follows:

$$\begin{aligned}\bar{i}_{L1k}&=D_k\bar{i}_{L1k\_sh}+(1-D_k)\bar{i}_{L1k\_nsh}\\&=D_k i_{PVk}+\frac{\hat{i}_s(1-D_k)\hat{v}_{Hk}}{2\hat{v}_{DCk}(1-2D_k)}.\end{aligned} \tag{16}$$

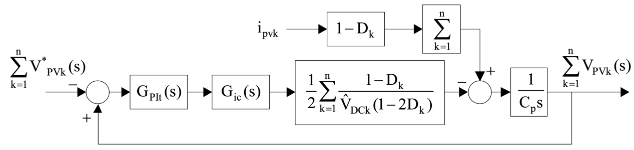

Figure 4. Block diagram of the total PV voltage loop.

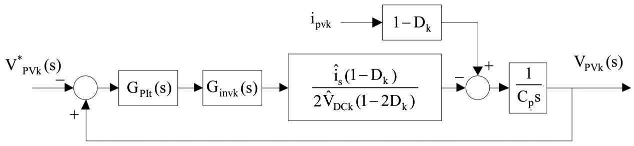

Figure 5. Block diagram of the separate PV voltage loop.

In addition, a PI controller $G_{PIt}(s)=k_{Pt}+\frac{k_{It}}{s}$ is used to track the total reference voltage coming from MPPT. The block diagram of the total PV array voltage loop is shown in Figure 4. Also, for modules 2 to n, a PI controller $G_{PIk}(s)=k_{Pk}+\frac{k_{It}}{s}$ is applied to separate PV voltage to achieve their own MPPTs. The block diagram of the separate PV array voltage loop is shown in Figure 5.

3.2. Independent DC-link voltage control using ANN

Artificial neural network is a model which is inspired from the biological neurons. It has a series of nodes with interconnections where mathematical functions and bias factors are applied to do an input/output mapping. An important feature of ANN that makes it proper for this kind of problems is its flexibility to lead in its domain and outside it, as well as work with the non-linear nature of the problem [18]. Although the data set for the ANN training is not complete and possibly all combinations are not considered, the ANN will be able to interpolate and extrapolate the results. These features make ANN a good and reliable choice for use as a controller.

Generally, the computational speed of ANN is high, because only simple mathematical functions apply to each layer. The ANN topology, which is used in this paper, is shown in Figure 1(b). It is a feed-forward structure which has three layers. The first layer has 20 neurons and also, second layer has 10 neurons. The number of neurons in the output layer is equal to the number of outputs. This topology has

$$\begin{aligned}G_{ic}&=\frac{I_s(s)}{I_s^*(s)}=\frac{G_{PRi}(s)G_f(s)G_{inv}(s)}{1+G_{PRi}(s)G_f(s)G_{inv}(s)}\\&=\frac{\hat{V}_{DCk}\left(k_{iP}S^2+k_{ip}\omega_0^2+k_{iR}\omega_0\right)}{L_f s^3+(r_f+\hat{V}_{DCk}k_{ip})s^2+L_f\omega_0^2 s+\hat{V}_{DCk}k_{ip}\omega_0^2+\hat{V}_{DCk}k_{iR}\omega_0+r_f\omega_0^2}\end{aligned} \tag{11}$$

Box I

tangent-sigmoid activation function hidden layers and, also, a linear activation function output layer. This ANN takes the real value of PV array voltages values as inputs and gives the shoot-through duty ratios for the control system as outputs. If the range of PV array voltage variation is considered 110 to 130 V and a step of 1V for its variation, then we have 21 points for each array leading to a data-set of a size equal to 213. For input data, the output of the ANN, which is the shoot-through duty ratio of PV modules, is calculated by using Eq. (2). After determining the inputs and outputs, the back propagation learning algorithm can be used for ANN training [19].

4. Design of PI controller parameters using particle swarm optimization

The PI is a well-known controller for industrial processes. This is due to its good performance and simple structure in a wide range of operating conditions. Tuning such a controller requires specification of two parameters: proportional gain K_p and integral gain K_i [20]. In the past, this problem has been solved by a trial and error technique. In this paper, the problem of PI parameters tuning is formulated as an optimization problem. The problem formulation employs four performance indexes, i.e. the overshoot, settling time, rise time, and integral absolute error of the step response as the objective function terms to tune the PI parameters for getting the best performance in a given plant. In this study, the primary design goal is to obtain good steady state response by minimizing the integral absolute error. At the same time, the transient response is guaranteed by minimizing the overshoot, settling time, and rise time of the step response. For solving this optimization problem, the particle swarm optimization algorithm is used in this paper.

The PSO is a stochastic optimization technique which uses swarming behaviors observed in flock of birds. In fact, the PSO was inspired by the sociological behavior associated with swarms. PSO was developed by James Kennedy and Russell Eberhart in 1995 as a new heuristic method [21]. It uses a number of particles that constitute a swarm moving around in one N-dimensional search space looking for the best position. The individuals in the swarm are called particles. Each particle in the PSO algorithm is a potential solution for the optimization problem and keeps track of its coordinates in the problem space and tries to search for the best position through flying in a multidimensional space, which are associated with the best solution (called best fitness) it has achieved so far and is called "*pbest*". Another "*best*" value called "*gbest*", that is tracked by the global version of the particle swarm optimizer, is the overall best value and its location obtained so far by each particle in the swarm. The sociological behavior, which is modeled in the PSO, is used to guide the particles. Each particle is determined by two vectors in the N-dimensional search space: The position vector and the velocity vector [22]. Each particle investigates its search space through previous experience, its present velocity, and the experience of the neighboring particles. The PSO concept is the change in the velocity of each particle toward its pbest and gbest positions at each iteration. In the PSO, acceleration of each particle is weighted by a random term [23]. PSO is a history-based algorithm such that in each iteration, particles use their own behavior associated with the previous iterations. Let X and V denote the particle's position vector and its corresponding velocity vector in the search space. In this algorithm, at iteration h, each particle i has its position defined by $X_i^h = [X_{i,1}, X_{i,2}, ..., X_{i,N}]$ and also, its velocity vector defined by $V_i^h = [V_{i,1}, V_{i,2}, ..., V_{i,N}]$ in the search space. In the next iteration, position and velocity of each particle can be calculated as:

$$\begin{aligned} V_{i,n}^{h+1} &= W \times V_{i,n}^h + C_1 \times \mathrm{rand}_1 \times \left(p\mathrm{best}_{i,n} - X_{i,n}^h\right) \\ &\quad + C_2 \times \mathrm{rand}_2 \times \left(g\mathrm{best}_n - X_{i,n}^h\right), \\ i &= 1, 2, ..., m, \qquad n = 1, 2, ..., N, \end{aligned} \tag{17}$$

$$\begin{aligned} X_{i,n}^{h+1} &= X_{i,n}^h + V_{i,n}^{h+1} \quad \text{if} \;\; X_{\min,i,n} \le X_1^{h+1} \le X_{\max,i,n}, \\ &= X_{\min,i,n} \qquad \text{if} \;\; X_{i,n}^{h+1} < X_{\min,i,n}, \\ &= X_{\max,i,n}p \qquad \text{if} \;\; X_{i,n}^{h+1} > X_{\max,i,n}. \end{aligned} \tag{18}$$

The transient response is very important, therefore, both the overshoot and time duration of the transient response must be kept within tolerable limits. Hence, four indexes of the transient response are utilized to characterize the performance of PI control systems.

The objective function (f_{Total}) for optimal design of PI controller parameters can be formulated as follows:

$$f_{\mathrm{Total}} = f_o + f_{RT} + f_{ST} + f_{IAE}, \tag{19}$$

where f_o, f_{RT}, f_{ST} and f_{IAE} are the overshoot, rise time, settling time, and integral absolute error of the step response, respectively. To apply PSO for tuning the PI controller parameters, the closed-loop transfer function of the total PV voltage loop and separate PV voltage loop are necessary. These closed-loop transfer functions which are calculated using block diagram of Figures 4 and 5, are included in Appendix A. Also, the parameters used in PSO are given in Appendix B.

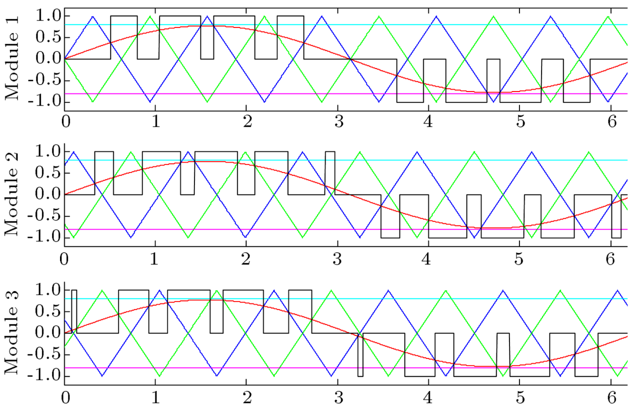

Figure 6. Modulation scheme for the proposed system.

5. The PS-SPWM for QZS-CMI

The modulation technique applied in the proposed system is a phase shifted sinusoidal pulse width modulation which is shown in Figure 6. The shoot-through states are inserted by the simple boost control method [16]. In this control method, two straight lines, which are denoted as $1 - D_n$ and $D_n - 1$, envelops equal to or greater than the peak value of the sinusoidal reference signals are used to control shoot-through duty ratio. If the triangular carrier signal is smaller than $D_n - 1$ or bigger than $1 - D_n$, the two switches of one leg in H-bridge module are turned on simultaneously. In PS-SPWM schemes, the number of triangular carrier waves is equal to $m - 1$, where m is equal to level number. Also, the required phase shifts among different carriers is given as:

$$\varphi = \frac{360°}{m-1}. \tag{20}$$

Therefore, in this case ($m = 7$), triangular carriers of different H-bridge modules are shifted 60° with respect to each other.

6. Simulation results

Performance evaluation of the proposed control strategy was carried out by simulation in PSCAD/EMTDC software. The parameters of QZS-CMI are shown in Table 1. Also, the codes of PSO algorithm are written in MATLAB for the best results to be obtained for the control parameters. As mentioned earlier, the closed-loop transfer function of the total PV voltage control loop and the separate PV voltage control loop are used for the optimization problem. The results of the PSO algorithm are shown in Table 2. Effectiveness of the proposed method is shown by comparing the results of the new proposed method with the results of [2] in Table 3. In this table, the overshoot, settling time, rise time, and integral absolute error of the step response for these closed-loop transfer functions are given. As shown in this table, the overshoot, settling time, rise time, and integral absolute error of step response for all the closed-loop transfer functions, obtained using PSO algorithm, are smaller than the results of [2]. Also, the nntool toolbox in MATLAB is used for ANN training.

Table 1. QZS-CMI parameters.

QZS-CMI parameters	Value
QZS inductance, L_1 and L_2	1.8 mH
QZS capacitance, C_1 and C_2	3300 μF
PV array parallel capacitance, C_p	1100 μF
Filter inductance, L_f	1 mH
Carrier frequency, f_c	5 kHz
Grid voltage	220V/50 Hz

Table 2. The parameters of the control system obtained by PSO algorithm.

Parameters	Value	Parameters	Value
k_{iP}	0.00491	k_{iR}	-0.01673
k_{Pt}	1.1511	k_{It}	1.5348
k_{Pk}	0.0263	k_{Ik}	0.0017

The P-V characteristic of the PV array is shown in Figure 7. The measured voltage and current for each PV array are used to apply the MPPT search algorithm for determining the PV voltage reference at the MPP. Incremental conductance algorithm is used for tracking the maximum power point of a PV array in this paper [24].

At first, all modules are working at 1000 W/m^2 and 25°C conditions and all the initial voltage references of MPPT algorithm are given at 120 V. The peak value of DC-link voltage in all modules is controlled at 145V. After 1 second, the third module's irradiation decreases to 700 W/m^2. Hence, according to Figure 7, the reference voltage of this module is decreases to about 119.2V by MPPT algorithm. It should be noted that the change of temperature mostly affects the voltage of maximum power point, so that temperature

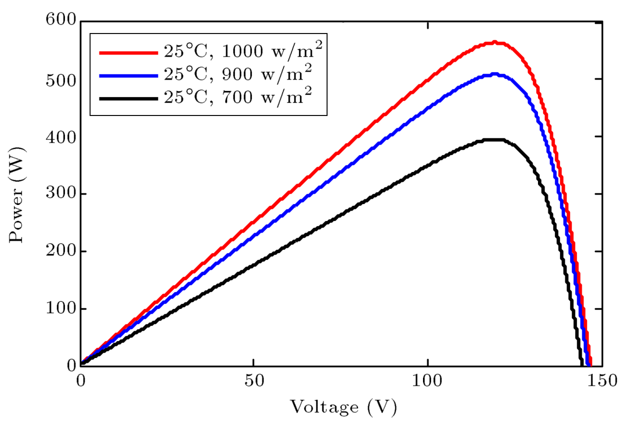

Figure 7. PV array power-voltage characteristic.

Table 3. Comparison of the results of the new proposed method with the results of [2].

Transfer functions	Overshoot (%)		Settling time (sec)		Rise time (sec)		Integral absolute error	
	Using controller parameters obtained by PSO	Using controller parameters in [2]	Using controller parameters obtained by PSO	Using controller parameters in [2]	Using controller parameters obtained by PSO	Using controller parameters in [2]	Using controller parameters obtained by PSO	Using controller parameters in [2]
Total PV voltage loop	8.62	56.1	0.362	2.84	0.0395	0.177	0.0384	0.5052
Separate PV voltage loop	12.9	33.3	0.438	0.511	0.0578	0.0651	0.0584	0.0988

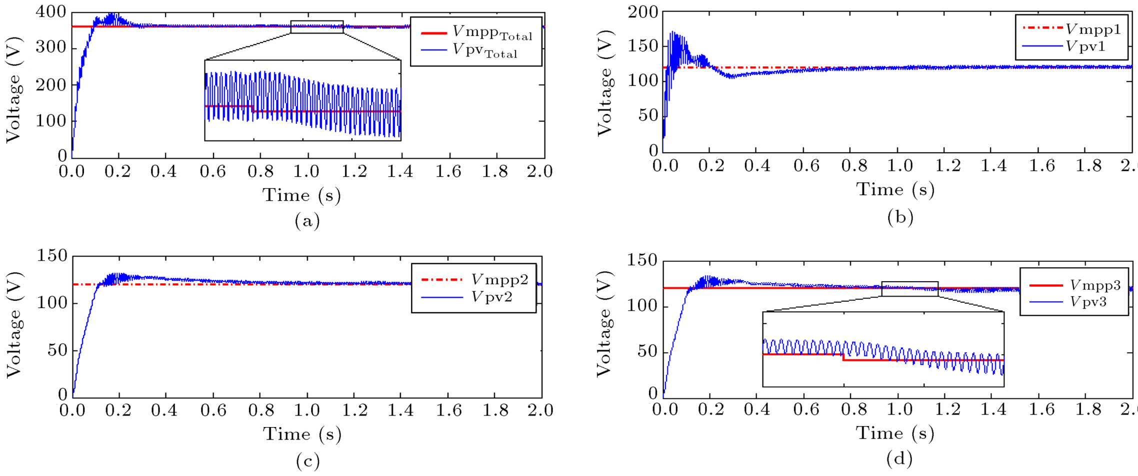

Figure 8. Simulation results: (a) Total PV array voltage; (b) PV array voltage of the first module; (c) PV array voltage of the second module; and (d) PV array voltage of the third module.

rising causes the voltage of maximum power point to drop. While, the change of solar irradiation mainly affects the current injection.

The total PV voltage (sum of all three PV array voltages) and other PV array voltages are shown in Figure 8(a)-(d), respectively. It can be seen that during the change in the MPPT reference value due to the change in environmental condition, the proposed control method has excellent tracking performance after a very short transient. It can be seen in Figure 8(d) that after a change in the environmental condition of third module, the controller of this module tracks the new reference. As shown in Figure 8(b)-(d), PV array voltage of the first module is different with respect to the second and third modules. This is due to the fact that the modulation signal generation of the first module is different from that of other modules.

The inverter output voltage is shown in Figure 9. It can be indicated that the solar irradiation or temperature does not affect the seven-level staircase output voltage of the inverter due to shoot-through operation. It is no matter if the temperature and the solar irradiation change or not; the QZS-CMI always

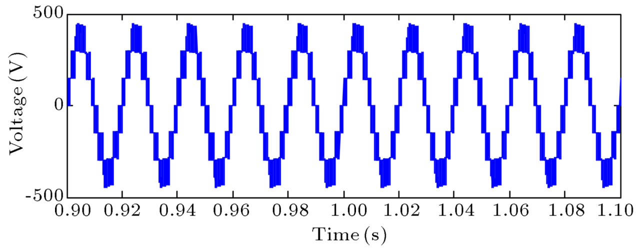

Figure 9. Inverter output voltage.

outputs a constant voltage which verifies the voltage balancing capability.

Figure 10 shows the grid-injected current which is exactly in phase with the grid voltage and ensures unity power factor. It should be noted that lower irradiation causes reduction of the grid-injected current. The DC-link voltage of the third module is shown in Figure 11. Low DC-link peak voltage fluctuation is because of capacitor voltages fluctuation due to inverter status change from the shoot-through mode to non-shoot-through mode and vice versa. It can be seen that with the ANN, DC-link peak voltages are kept at the reference value (145 V). It should be noted that,

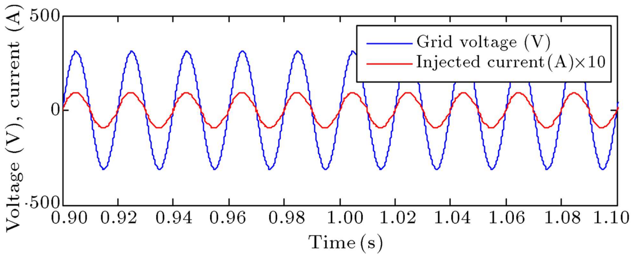

Figure 10. Grid voltage and current.

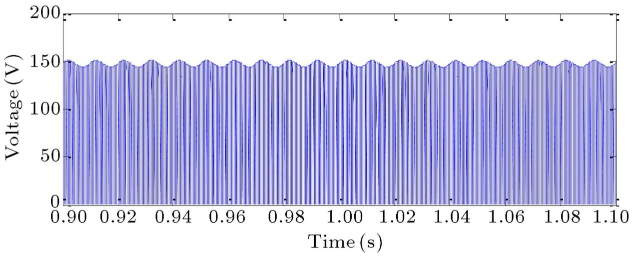

Figure 11. DC-link voltage of the third module.

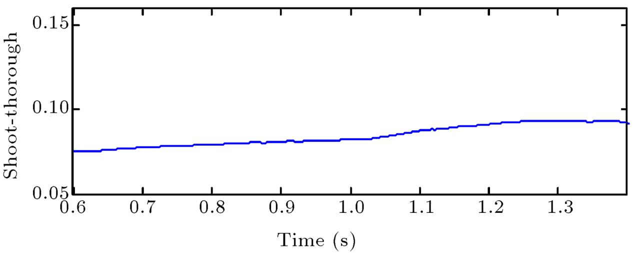

Figure 12. Shoot-through duty ratio of the third module.

according to Eq. (2), after decrement of the reference voltage of the third module by MPPT algorithm, longer shoot-through time interval is necessary for this module to fix the DC-link peak voltage at 145 V. The shoot-through duty ratio of third module, during the change in the MPPT reference value, is shown in Figure 12. As shown in this figure, ANN adjusts new shoot-through duty ratio after a very short transient, so that third module's DC-link peak voltage has a very low distortion after a change in the solar irradiation.

7. Conclusion

In this paper, a new control method for QZS-CMI based single-phase grid-connected PV system is proposed. The proposed system is a combination of QZSI and CHB multilevel topology and has both of their advantages. This enables independent MPPT control for each PV array in different conditions. Moreover, independent DC-link voltage control enforces all QZS-HBI modules to have balanced voltages and, also, grid-injected current is fulfilled at unity power factor. The control parameters are designed using PSO algorithm. It was shown that the system has fast and accurate response. Also, an ANN used for DC-link voltage control has some advantages such as simplicity, cost reduction, fast response, and more reliability. Performance of the proposed control system for a seven level QZS-CMI is evaluated under variable environment conditions. The simulation results show the effectiveness of the proposed control strategy for a QZS-CMI based single-phase grid-connected PV system.

References

1. Sastry, J., Bakas, P., Kim, H., Wang, L. and Marinopoulos, A. "Evaluation of cascaded H-bridge inverter for utility-scale photovoltaic systems", *Renewable Energy*, **69**(1), pp. 208-218 (2014).

2. Liu, Y., Ge, B., Abu-Rub, H. and Peng, F.Z. "An effective control method for quasi-Z-source cascade multilevel inverter-based grid-tie single-phase photovoltaic power system", *IEEE Transactions on Industrial Informatics*, **10**(1), pp. 399-407 (2014).

3. Liu, Y., Ge, B., Abu-Rub, H. and Sun, D. "Comprehensive modeling of single-phase quasi-Z-source photovoltaic inverter to investigate low-frequency voltage and current ripple", *IEEE Transactions on Industrial Electronics*, **62**(7), pp. 4194-4202 (2015).

4. Patidar, K. and Umarikar, A.C. "High step-up pulse-width modulation DC-DC converter based on quasi-Z-source topology", *IET Power Electronics*, **8**(4), pp. 477-488 (2015).

5. Liu, S., Ge, B., Jiang, X., Abu-Rub, H. and Peng, F.Z. "Comparative evaluation of three Z-source/quasi-Z-source indirect matrix converters", *IEEE Transactions on Industrial Electronics*, **62**(2), pp. 692-701 (2015).

6. Peng, F.Z. "Z-source inverter", *IEEE Transactions on Industry Applications*, **39**(2), pp. 504-510 (2003).

7. Loh, P.C., Vilathgamuwa, D.M., Lai, Y.S., Chua G.T. and Li, Y. "Pulse-width modulation of Z-source inverters", *IEEE Transactions on Power Electronics*, **20**(6), pp. 1346-1355 (2005).

8. Miaosen, S., Joseph, A., Jin, W., Peng, F.Z. and Adams, D.J. "Comparison of traditional inverters and Z -source inverter for fuel cell vehicles", *IEEE Transactions on Power Electronics*, **22**(4), pp. 1453-1463 (2007).

9. Yuan, L., Anderson, J., Peng, F.Z. and Dichen, L. "Quasi-Z-source inverter for photovoltaic power generation systems", *Applied Power Electronics Conference and Exposition (APEC 2009)*, pp. 918-924 (2009).

10. Nguyen, M., Jung, Y. and Lim, Y. "Single-phase AC-AC converter based on quasi-Z-source topology", *IEEE Transactions on Power Electronics*, **25**(8), pp. 2200-2210 (2010).

11. Colak, I., Kabalci, E. and Bayindir, R. "Review of multilevel voltage source inverter topologies and con-

trol schemes", *Energy Conversion and Management*, **52**(2), pp. 1114-1128 (2011).

12. Liu, Y. Abu-Rub, H. Ge, B. and Peng F.Z. "Phase-shifted pulse-width-amplitude modulation for quasi-Z-source cascade multilevel inverter based PV power system", *Energy Conversion Congress and Exposition (ECCE)*, pp. 94-100 (2013).
13. Shajith, A. and Kamaraj, V. "Bipolar multicarrier PWM techniques for cascaded quasi-Z-source multilevel inverter", *Circuits, International Conference on Power and Computing Technologies (ICCPCT 2013)*, pp. 236-240 (2013).
14. Sun, D., Ge, B., Yan, X., Bi, D., Zhang, H., Liu, Y., Abu-Rub, H., BenBrahim, L. and Peng, F.Z. "Modeling, impedance design, and efficiency analysis of quasi-Z-source module in cascade multilevel photovoltaic power system", *IEEE Transactions on Industrial Electronics*, **61**(11), pp. 6108-6117 (2014).
15. Liu, Y., Abu-Rub, H., Ge, B. and Peng, F.Z. "Impedance design of 21-kW quasi-Z-source H-bridge module for MW-scale medium-voltage cascaded multilevel photovoltaic inverter", *International Symposium on Industrial Electronics (ISIE 2014)*, pp. 2490-2495 (2014).
16. Sun, D., Ge, B., Peng, F., Abu-Rub, H., Bi, D. and Liu, Y. "A new grid-connected PV system based on cascaded H-bridge quasi-Z source inverter", *IEEE International Symposium on Industrial Electronics (ISIE 2012)*, pp. 951-956 (2012).
17. Zmood, D. and Holmes, D. "Stationary frame current regulation of PWM inverters with zero steady-state error", *IEEE Transactions on Power Electronics*, **18**(3), pp. 814-822 (2003).
18. Bose, B. "Neural network applications in power electronics and motor drives - An introduction and perspective", *IEEE Transactions on Industrial Electronic*, **54**(1), pp. 14-33 (2007).
19. Karnin, E. "A simple procedure for pruning back-propagation trained neural networks", *IEEE Transactions on Neural Networks*, **1**(2), pp. 239-242 (1990).
20. Hsiao, Y., Chuang, C. and Chien, C. "Ant colony optimization for designing of PID controllers", *IEEE International Symposium on Computer Aided Control Systems Design*, pp. 321-326 (2004).
21. Kennedy, J. and Eberhart, R. "Particle swarm optimization", *IEEE International Conference on Neural Networks*, pp. 1942-1948 (1995).
22. Taghizadeh, H. and Hagh, M.T. "Harmonic elimination of cascade multilevel inverters with nonequal DC sources using particle swarm optimization", *IEEE Transactions on Industrial Electronics*, **57**(11), pp. 3678-3684 (2010).
23. Clerc, M. and Kennedy, J. "The particle swarm - explosion, stability, and convergence in a multidimensional complex space", *IEEE Transactions on Evolutionary Computation*, **6**(1), pp. 58-73 (2002).
24. Salas, V., Olıas, E., Barrado, A. and Lázaro, A. "Review of the maximum power point tracking algorithms for stand-alone photovoltaic systems", *Solar Energy Materials and Solar Cells*, **90**(11), pp. 1555-1578 (2006).

Appendix A

Closed-loop transfer functions are calculated using block diagram of Figures 4 and 5 as shown in Box II.

Appendix B

The parameters used in PSO algorithm is shown in Table B.1.

$$\frac{\sum V_{PVk}}{\sum V^*_{PVk}}$$

$$= \frac{\left[k_{Pt}k_{iP}s^3 + k_{It}k_{iP}s^2 + k_{Pt}(k_{iP}\omega_0^2 + k_{iR}\omega_0)s + k_{It}\left(k_{iP}\omega_0^2 + k_{iR}\omega_0\right)\right] \times \left(\frac{1-D_1}{2(1-2D_1)} + \frac{1-D_2}{2(1-2D_2)} + \frac{1-D_3}{2(1-2D_3)}\right)}{C_P L_f s^5 + C_P(\hat{V}_{DC}k_{iP} + r_f)s^4 + \left(C_P L_f\omega_0^2 + k_{Pt}k_{iP} \times (\frac{1-D_1}{2(1-2D_1)} + \frac{1-D_2}{2(1-2D_2)} + \frac{1-D_3}{2(1-2D_3)})\right)s^3 +} \tag{A.1}$$

$$+ \left(C_P(\hat{V}_{DC}k_{ip}\omega_0^2 + \hat{V}_{DC}k_{iR}\omega_0 + r_f\omega_0^2) + k_{It}k_{iP}\left(\frac{1-D_1}{2(1-2D_1)} + \frac{1-D_2}{2(1-2D_2)} + \frac{1-D_3}{2(1-2D_3)}\right)\right)s^2 +$$

$$+ k_{Pt}\left(k_{iP}\omega_0^2 + k_{iR}\omega_0\right)\left(\frac{1-D_1}{2(1-2D_1)} + \frac{1-D_2}{2(1-2D_2)} + \frac{1-D_3}{2(1-2D_3)}\right)s$$

$$+ k_{It}\left(k_{iP}\omega_0^2 + k_{iR}\omega_0\right)\left(\frac{1-D_1}{2(1-2D_1)} + \frac{1-D_2}{2(1-2D_2)} + \frac{1-D_3}{2(1-2D_3)}\right)$$

$$\frac{V_{PVk}}{V^*_{PVk}} = \frac{k_{Pk}\left(\frac{1-D_k}{1-2D_k}\right)\frac{i_s}{2}s + k_{Ik}\left(\frac{1-D_k}{1-2D_k}\right)\frac{i_s}{2}}{C_P s^2 + k_{Pk}\left(\frac{1-D_k}{1-2D_k}\right)\frac{i_s}{2}s + k_{Ik}\left(\frac{1-D_k}{1-2D_k}\right)\frac{i_s}{2}} \tag{A.2}$$

Box II

Table B.1. PSO parameters.

Particle no	100
NPar	5
MaxIter	80
w	0.9
KEI	0.1
n1	2
n2	2

Biographies

Ali Akhavan was born in Kashan, Iran in 1990. He received the BSc and MSc degrees in Electrical Engineering from the University of Kashan, Kashan, Iran, in 2012 and 2014, respectively. He is currently working toward the PhD degree in Electrical Engineering, in the University of Kashan. His research interests include power electronics, renewable energy power generation, power quality, and microgrids.

Hamid Reza Mohammadi was born in Qom, Iran. He received the BSc degree in Electrical Engineering from Sharif University of Technology, Tehran, Iran, in 1993, the MSc degree in Electrical Engineering from the University of Tabriz, Tabriz, Iran, in 1995, and the PhD degree in Electrical Engineering from Tarbiat Modares University, Tehran, in 2008. His research interests include power quality, digital signal processing, and power electronics.